



Evaluating night-time light sources and correlation with socio-economic development using high-resolution multi-spectral Jilin-1 satellite imagery of Quito, Ecuador

C. Scott Watson, John R. Elliott, Marco Córdova, Jonathan Menoscal & Santiago Bonilla-Bedoya

To cite this article: C. Scott Watson, John R. Elliott, Marco Córdova, Jonathan Menoscal & Santiago Bonilla-Bedoya (2023) Evaluating night-time light sources and correlation with socio-economic development using high-resolution multi-spectral Jilin-1 satellite imagery of Quito, Ecuador, International Journal of Remote Sensing, 44:8, 2691-2716, DOI: [10.1080/01431161.2023.2205983](https://doi.org/10.1080/01431161.2023.2205983)

To link to this article: <https://doi.org/10.1080/01431161.2023.2205983>



© 2023 The Author(s). Published by Informa UK Limited, trading as Taylor & Francis Group.



Published online: 05 May 2023.



[Submit your article to this journal](#)



Article views: 445





[View related articles](#)



[View Crossmark data](#)

Evaluating night-time light sources and correlation with socio-economic development using high-resolution multi-spectral Jilin-1 satellite imagery of Quito, Ecuador

C. Scott Watson ^a, John R. Elliott^a, Marco Córdova^b, Jonathan Menoscal^b and Santiago Bonilla-Bedoya ^c

^aCOMET, School of Earth and Environment, University of Leeds, Leeds, UK; ^bFacultad Latinoamericana de Ciencias Sociales, FLACSO, Quito, Ecuador; ^cResearch Center for the Territory and Sustainable Habitat, Universidad Tecnológica Indoamérica, Machala y Sabanilla, Ecuador

ABSTRACT

Artificial light at night (ALAN) has positive and negative effects on social, economic, environmental, and ecological systems, and will increase with urban expansion. In this study, we used a multi-spectral 1.5 m resolution night-time acquisition from a Jilin-1 satellite over the city of Quito, Ecuador, to evaluate spatial lighting patterns in an expanding and topography complex-built environment. We demonstrated a requirement for robust georeferencing and orthorectification due to the complex topography, with errors on the order of 4–6 pixels (5.8–8.4 m CE95). We also quantified differences in observed brightness due to the image acquisition and local geometry. Street light type was distinguishable between high-pressure sodium (HPS) and light emitting diode (LED) sources (F1-score = 0.72–0.83) using a shark random forest decision tree approach. Additionally, street lights could be located within 10 m (F1-score = 0.71) with balanced omissions and commissions. Spatial trends revealed that the road network was the dominant source of illumination, accounting for 45% of illuminated pixels, whereas built-up areas accounted for 23%. Overall, 68% of all illuminated pixels were on or within 10 m of the road. Higher socio-economic development was associated with higher proportions of LED lighting, greater road network lighting and density of street lights, higher overall radiance for built-up areas and the road network, and greater coverage and illumination of designated green spaces. The broad impacts of ALAN mean that addressing the causes and consequences of lighting inequalities is a complex issue. Nonetheless, Jilin-1 night-time imagery offers a low-cost way to map and monitor light sources at high-resolution that will be beneficial to city-planners and progressing Sustainable Development Goals.

ARTICLE HISTORY

Received 3 March 2023
Accepted 16 April 2023

CONTACT C. Scott Watson  c.s.watson@leeds.ac.uk  COMET, School of Earth and Environment, University of Leeds, LS2 9JT, UK

© 2023 The Author(s). Published by Informa UK Limited, trading as Taylor & Francis Group.

This is an Open Access article distributed under the terms of the Creative Commons Attribution License (<http://creativecommons.org/licenses/by/4.0/>), which permits unrestricted use, distribution, and reproduction in any medium, provided the original work is properly cited. The terms on which this article has been published allow the posting of the Accepted Manuscript in a repository by the author(s) or with their consent.

Key policy highlights

- Image acquisition geometry affects the observed radiance and would require consideration when evaluating spatial and temporal trends.
- Jilin-1 night-time satellite imagery offers a low-cost mechanism to map and monitor light sources at high-resolution that is sufficient to identify individual sources such as street lights, buildings, and recreational spaces.
- Radiance intensity was correlated with the degree of socio-economic development. In the higher socio-economic classes, we observed higher proportions of LED lighting, greater road network lighting and density of street lights, higher overall radiance for built-up areas and the road network, and greater coverage and illumination of designated green spaces.

1. Introduction

Artificial light at night (ALAN) is now prevalent in built-up areas where buildings, street lights, and other anthropogenic sources emit light that is scattered and reflected into the atmosphere (Figure 1). ALAN is associated with potential benefits such as an improved perception of safety (Loewen, Daniel Steel, and Suedfeld 1993; Pedrosa et al. 2021), although associations between lighting and crime rates show mixed results (e.g. Steinbach et al. 2015; Welsh and Farrington 2008). Additionally, illuminated areas are long documented as a draw for economic activity, where lighting prolongs after sunset (Karekezi and Majoro 2002; Mellander et al. 2015; Bouman 1987). Night-time lights are also relevant to disaster risk reduction, where light disturbance and recovery can be monitored (Qiang, Huang, and Jinwen 2020; Wang et al. 2018) and community resilience to disaster events can be improved by designing safe spaces and evacuation routes with (solar) lighting (León and March 2016; French et al. 2019). However, exposure to ALAN is also associated with negative implications for public health (Navara and Nelson 2007; Touitou, Reinberg, and Touitou 2017; Keshet-Sitton et al. 2017) and biodiversity (Stone, Jones, and Harris 2012; Hölker et al. 2010; Giavi et al. 2020). The transition from high-pressure sodium (HPS) HPS to energy-efficient light emitting diode (LED) lighting, which illuminates over a broader range of wavelengths, could also further disrupt ecosystems (Davies and Smyth 2018; Pawson and Bader 2014). The wide impact of ALAN makes it a key consideration for sustainable urban growth, where night-time light sources should be designed considering the range of societal and natural impacts.

Night-time satellite images have measured ALAN for applications including urban development and electrification rates (Zhao et al. 2022; Min and Mensan Gaba 2014; Giacomo et al. 2020), poverty and economic activity (Bruederle and Hodler 2018; Doll Christopher, Muller, and Elvidge 2000; Mellander et al. 2015), disaggregating census population data (Lloyd, Sorichetta, and Tatem 2017; Tan et al. 2018), as a proxy for building volume (Shi et al. 2020; Peled and Fishman 2021), and disaster resilience and response (Qiang, Huang, and Jinwen 2020; Molthan and Jedlovec 2013). However, the number of studies using night-time satellite data was limited until the 1990s when the Defence Meteorological Satellite Program (DMSP) data became available in digital format (Levin et al. 2020). The spatial resolution of the available data was also limited to 100–

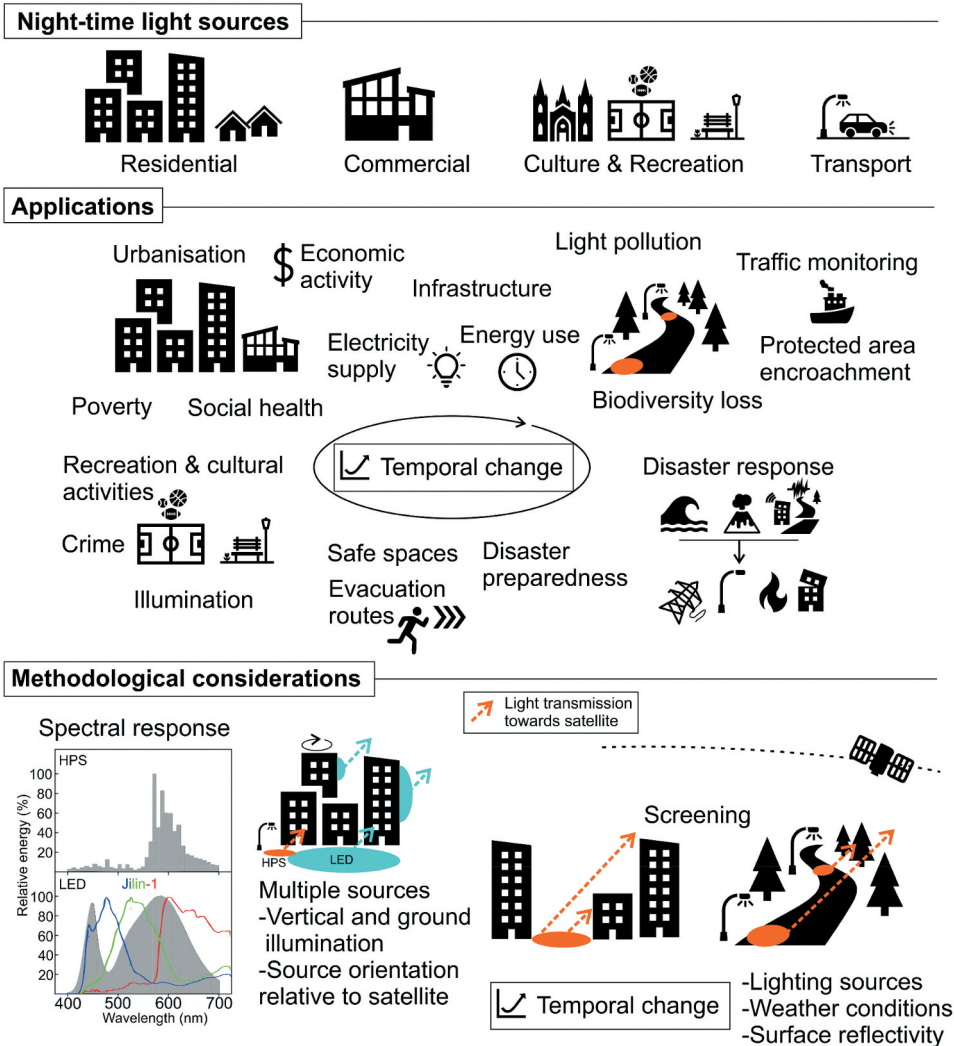


Figure 1. Sources, applications, and methodological considerations when using night-time light satellite imagery in a built environment. Illustrative spectral response plot shows light sources (high-pressure sodium and light-emitting diode) and Jilin-1 bands adapted from Pawson and Bader (2014) and Cheng et al. (2020) respectively.

1000 m until the launch of the commercial satellites EROS-B in 2013 and Jilin-1 (3B) in 2017 offering <2 m resolution night images (Levin et al. 2020; Noam et al. 2014). Nonetheless, several studies have shown correlations between coarse resolution night-time light distribution and socio-economic datasets such as population and economic development (Henderson, Storeygard, and Weil 2011; Elvidge et al. 2012; Sutton et al. 2001), therefore offering the potential for satellite-derived proxy censuses. However, the strength of the observed trends was highly variable between and within countries (Mellander et al. 2015; Henderson, Storeygard, and Weil 2011), and it is not known if similar trends are observed using higher-resolution datasets.

Nonetheless, night-time light data offer a valuable mechanism for monitoring Sustainable Development Goals (SDGs) including poverty (SDG 1), energy (SDG 7), inequalities (SDG 10), and sustainable cities and communities (SDG 11), particularly where informal settlements develop without state-provided infrastructure (Stokes and Seto 2019; Ivan et al. 2020).

Commercial satellites offer new opportunities for monitoring night-time lights at a resolution where individual sources of light, such as street lights and buildings, are resolvable (Cheng et al. 2020). For example, the recent availability of high-resolution multi-spectral night-time imagery from Jilin-1 creates new opportunities to quantify the spectral signature and therefore the type of light source, which is important as HPS sources are replaced with LEDs (Cheng et al. 2020). Therefore, this potentially enables analysis of socio-economic development and other variables at scales that are relevant to urban planners (Noam et al. 2014). However, using these higher resolution data requires greater consideration of confounding factors affecting the observed brightness due to the variable satellite viewing geometry, screening due to vegetation and buildings, the orientation of light sources in relation to the satellite, time of acquisition, moonlight illumination, and the lack of atmospheric corrections (Figure 1) (Levin et al. 2020; Guk and Levin 2020; Noam et al. 2014; Katz and Levin 2016).

In this study, we tasked a night-time acquisition from the Jilin-1 Gaofen-03C01 satellite (1.5 m resolution and 3 band RGB) over the city of Quito, Ecuador, with the aim of evaluating spatial lighting patterns in an expanding and topography complex-built environment. Our objectives were to (1) quantify differences in observed brightness due to image acquisition geometry, (2) evaluate street light typology classification using the multi-spectral Jilin-1 imagery and geopositioning accuracy, and (3) assess the spatial variation in brightness in relation to socio-economic and land cover characteristics, including the density of street lights.

2. Methods

2.1. Study site

Quito is located in central Ecuador at an altitude of 2,800 m and is bounded by steep topography, including Pichincha Volcano to the west (Figure 2). The city is expanding to the north, east, and south (Bonilla-Bedoya et al. 2020) (Figure 2a), which exposes populations to a range of natural hazards including landslides, floods, volcanic hazards, and earthquakes (Watson et al. 2022; Chatelain et al. 1999; Valcárcel et al. 2017; Hall et al. 2008). Westward expansion on the slopes of Pichincha is limited by designated protection following previous encroachment and the subsequent occurrence of debris flow and landslides (Vidal, Burgos, and Zevallos 2015). Informal settlements have traditionally formed on these slopes where natural hazard risk is greatest (Vidal, Burgos, and Zevallos 2015; Sierra 2009). The diversity of built-up areas over a range of rugged and flat topographies, combined with social inequalities, makes Quito a useful test case for night-time satellite imagery.

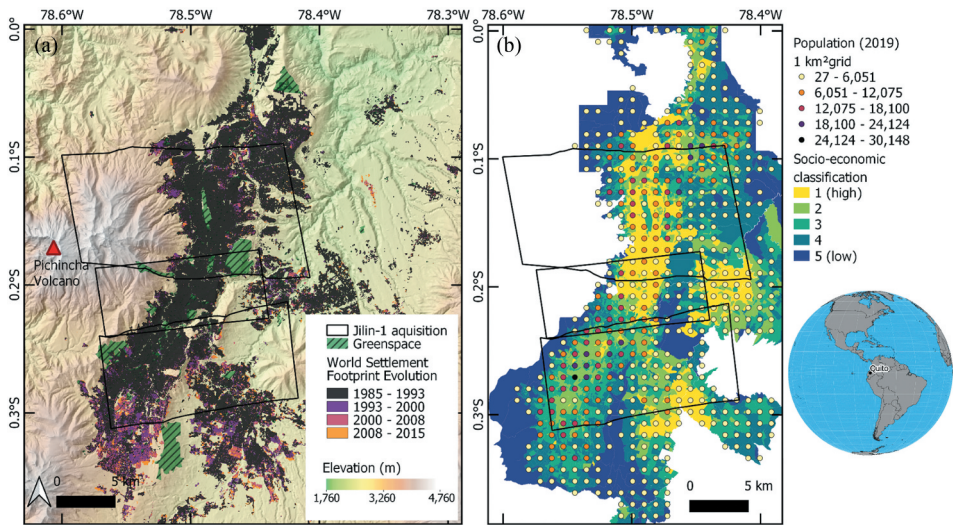


Figure 2. Study location overview of the city of Quito, Ecuador. (a) Footprints of the Jilin-1 night-time acquisitions overlaid on the urban expansion of Quito (1985–2015), which is shown from the World Settlement Footprint Evolution (WSF-Evo) dataset (Marconcini et al. 2020) with a hillshaded digital elevation model (DEM) background. Areas of green space are from Open Government data (<https://datosabiertos.Gob.ec/>, last accessed: 04 November 2022). (b) Total population gridded to 1 km² cells and socio-economic classification data (CIUQ 2020; Instituto Geográfico Militar 2019).

Table 1. Acquisition and processing parameters of the Jilin-1 GaoFen-03 multi-spectral imagery, listed in order of acquisition time on the 8 July 2021.

Image ID	Roll/Pitch/ Yaw	Satellite azimuth/Satellite elevation	Orthorectification errors (m). CE95/LE95*
[1] JL1GF03C01_MSS_20210708102944_200054991_102_0069_001_L1A_MSS	-2.02/30.92/ 0.55	176.39/56.08	8.4/5.2
[2] L1GF03C01_MSS_20210708103041_200054991_105_0210_001_L1A_MSS	-5.09/-7.58/ 0.33	317.02/80.56	5.8/7.5
[3] JL1GF03C01_MSS_20210708103138_200054991_108_0354_001_L1A_MSS	-5.92/ 40.90/-2.24	343.46/44.80	7.6/5.9

*CE95 (horizontal error): circular standard error at 95% confidence. LE95 (vertical error): linear error at 95% confidence.

2.2. Jilin-1 night-time satellite imagery processing

Night-time satellite imagery from Jilin-1 (hereon: JL1-NT) GaoFen-03C01 satellite was acquired over Quito in three sequential acquisitions on 8 July 2021 at ~10:30 UTC (05:30 local time) with 100 ms exposure time (Table 1). The imagery covers 401 km² of Quito with 25.5 km² of overlap between the three acquisitions. The imagery was provided at Level 1A with rational polynomial coefficient (RPC) files, radiometric correction information, and metadata indicating cloud-free conditions, though details of how this was determined were not known. The imagery is 8-bit multi-spectral data with three bands: 580–730 nm (red), 490–580 nm (green), and 430–520 nm (blue), at ~1.2 m resolution (nadir) (EDAP 2022). The data are provided as digital numbers with per-band gain and offset calibration coefficients for conversion to radiance values (Table S1).

Georeferencing night-time satellite imagery is complicated by the visual difference between features in an optical satellite image compared to a night-time satellite imagery, where illumination patterns are derived from one or more sources of light. Additionally, the source and illumination angle of a light source creates a variable and dispersed area of illumination depending on the reflecting surface, which is further complicated by off nadir

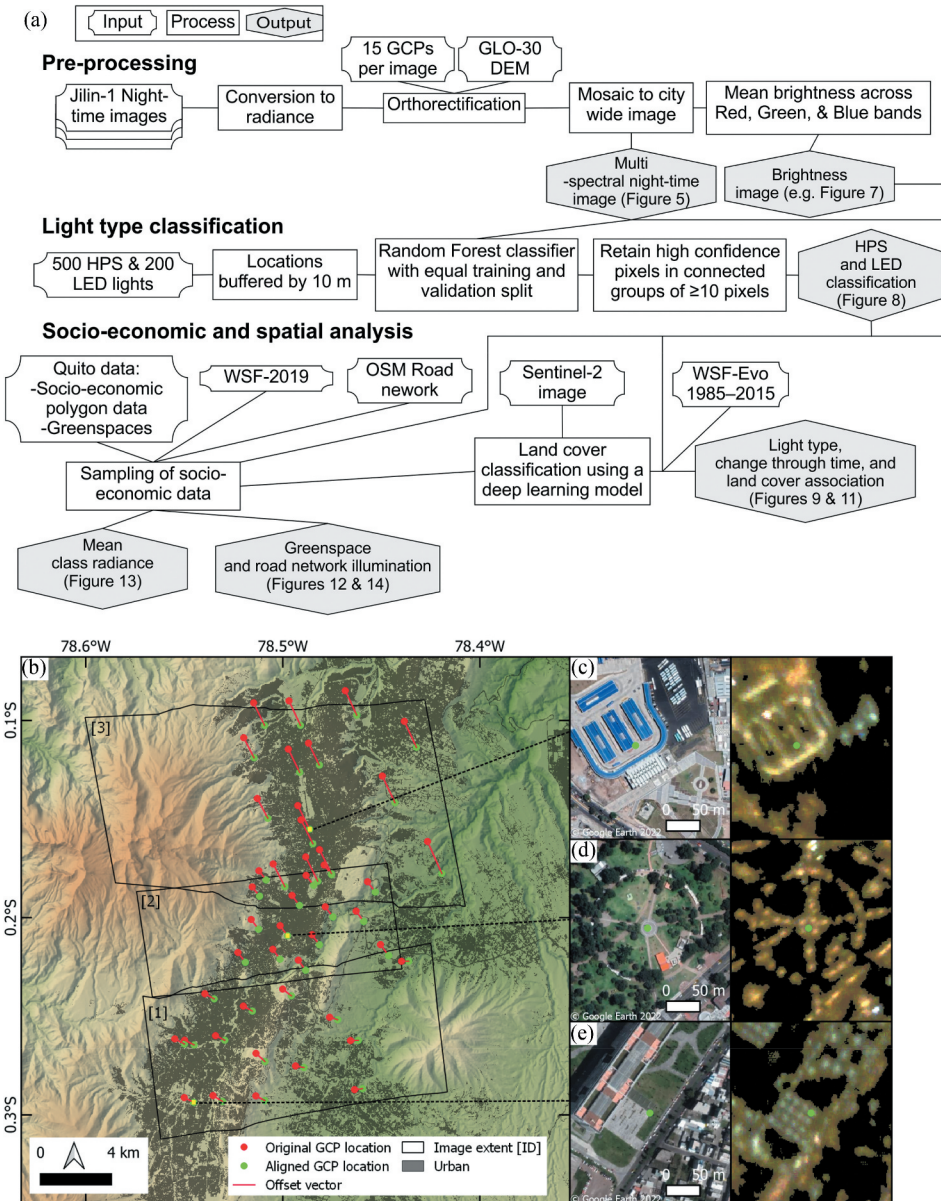


Figure 3. (a) Jilin-1 night-time satellite acquisition processing. (b) Image IDs and footprints (Table 1) and the location of GCPs used to orthorectify each image. Offsets show the initial image georeferencing provided by the RPCs. (c – e) Examples of features used as GCP locations with optical satellite imagery (left panel) and corresponding Jilin-1 night-time imagery (right panel).

viewing angles of the satellite that can obscure or distort the apparent light sources. Therefore, we identified 15 ground control points (GCPs) for georeferencing in each image using illuminated features such as buildings, path networks, and car parks, and assigned latitude and longitude positions using Google Satellite Basemap imagery (Figure 3). The GCP elevation values were derived from the Copernicus 30 m digital elevation model (DEM) (GLO-30) (Airbus Defence and Space GmbH 2020), accounting for the geoid-ellipsoid difference (EGM2008: mean of 26.98 ± 0.1 m). The GCPs revealed an initial horizontal georeferencing offset for each image [1–3] of 556 ± 83 m, 701 ± 25 m, and $1,429 \pm 280$ m, respectively (Figure 3). We tested two methods to georeference the imagery, which are detailed in the following sections.

2.2.1. Jilin-1 imagery georeferencing using a road network

The first georeferencing method followed a workflow presented by Schwind and Storch (2022), which was designed to georeference astronaut night-time imagery from the International Space Station. Briefly, the method used the OpenStreetMap (OSM) road network (Contributors 2022) as a reference image, and keypoint matching were used to identify the tie points of the night-time images. These tie points were used to apply a polynomial transformation to rectify the night-time images to the OSM road network. The rectification was expected to perform best over lower gradient, illuminated urban areas since the method relies on the tie point matching and did not use a sensor model or DEM to guide the rectification.

2.2.2. Jilin-1 imagery orthorectification

The second georeferencing method used the JL1-NT image RPC model and 15 GCPs in each image to orthorectify the imagery using the RPC Orthorectification workflow in ENVI 5.6.1. Each image was orthorectified using the GLO-30 m DEM. The images were output in the UTM 17S coordinate system with bilinear resampling to 1.5 m resolution. The image row and column ground sampling distances reported in the metadata ranged from 1.23 to 2.11 m and 1.22 to 1.6 m, respectively.

Digital number (DN) values were converted to radiance (L) using the per band (b) gain and bias radiometric calibration coefficients (Table S1; Equation (1)):

$$L_b = (DN_b \times Gain_b) + Bias_b \quad (1)$$

The three acquisitions were mosaicked together into one image using the maximum pixel value in overlapping areas. Additionally, we derived a mean brightness dataset (JL1-mean) by taking the mean radiance value of the red, green, and blue (RGB) bands (e.g. Guk and Levin 2020).

2.3. Light type and street light classification

Cheng et al. (2020) demonstrated the use of Jilin-1 night-time imagery to classify and extract street lights over a 51 km^2 low gradient area of Shanghai where street lights were the dominant source of illumination. We applied a similar approach to our Quito imagery to map light locations and type (HPS or LED), which were subsequently sampled using socio-economic data to determine the dominant lighting source and distribution of LED lighting (Section 2.4). Ground truth street light locations and type for 700 lights were

manually mapped using Google Earth imagery of Quito with reference to Streetview (dated 2014) (Figure S2). HPS lights ($n = 500$) were sampled across each of the three images, whereas the LED lights ($n = 200$) were only sampled in the central acquisition where the LED arrays were clearly distinguishable. Source type was assigned based on a visual inspection in the daytime imagery and were not confirmed in the field. This means that other light types could exist within these classes such as metal halide that would produce a similar spectral signature to LED (Zheng et al. 2018). Though covering a much larger area ($>13,000 \text{ km}^2$) than our study area, reporting from the electric utility company Empresa Eléctrica Quito suggests a breakdown of 92.3% HPS, 1.7% LED, and 6% other sources including mercury pressure lights (Galindo, Borge-Diez, and Icaza 2022; ARCONEL 2020). Therefore, our LED class is expected to include other sources of light.

2.3.1. Light type classification

The 700 street light locations were buffered by 10 m (radius) and intersected with the JL1 imagery (with background zero values removed) to train a Shark Random Forest Model implemented in Orfeo ToolBox (OTB) 7.1.0 in QGIS 3.16.16 using default parameters (maximum number of trees = 100, minimum size of the node for a split = 25). The model was then applied to the full JL1-NT Quito extent to classify light sources into HPS or LED classes. Since we could not validate street lighting in the field, we split the input training data (700 light sources) equally between validation and training and report common accuracy metrics including precision, recall, and F1-Score. High confidence pixels (confidence ≥ 0.9) in groups of at least 10 connected pixels were used as the final light source classification.

2.3.2. Street light location classification

The location of street lights were extracted by modifying the approach of Cheng et al. (2020), which improved the classification accuracy when applied to our study area. The modifications we implemented were to use the JL1-NT RGB band mean rather than sum, apply mean smoothing to the data, and use a smaller road buffer. We also did not consider potential illumination due to road traffic owing to the early morning night-time acquisition time (05:30).

JL1-mean data were clipped to an 8 m road buffer and a circular neighbourhood of 13 pixels (19.5 m) was used to extract the maximum radiance value, which was assigned as the street light location. This circular neighbourhood represented a compromise in the ability to distinguish individual sources since the mean light spacing in our training data were $31.3 \pm 10.2 \text{ m}$ for HPS sources and $10.4 \pm 4.1 \text{ m}$ for LEDs. Where multiple connected pixels shared the same maximum value in the neighbourhood, they were converted to polygon and the polygon centroid was used as the final street light location. The ground truth of 700 street light locations was used as validation data. We assumed a 10 m radius positional uncertainty to account for mis-location of the validation dataset and the fact that the area of maximum brightness is likely to be offset from the street light location. Detections falling within 10 m of a validation point were classed as valid (true positive) and were evaluated alongside omissions (false negative) and commissions (false positive), which were used to derive the F1 accuracy score. The classified street light locations were buffered by 10 m and intersected with the light-type classification to find the majority class, which was assigned as the light type.

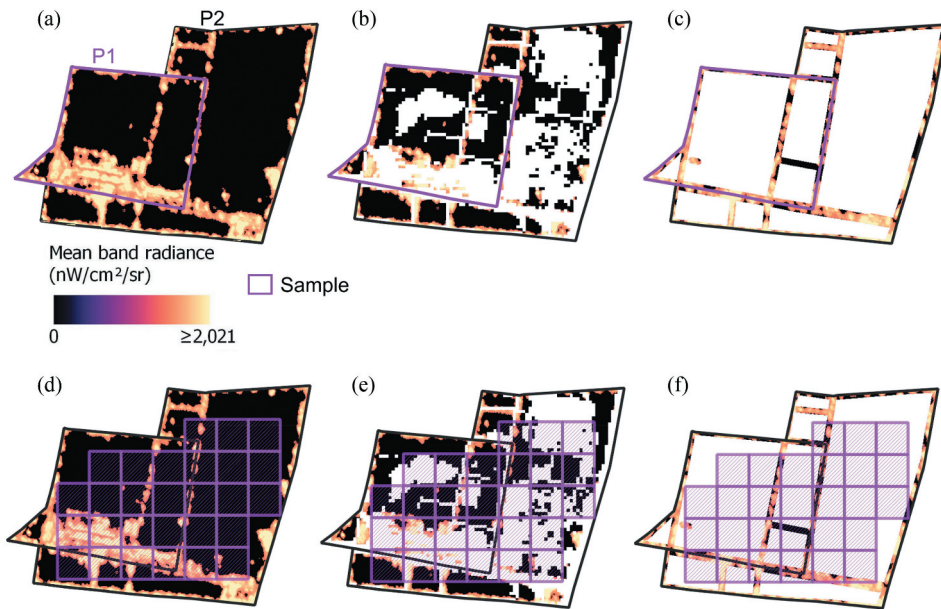


Figure 4. Two approaches used to sample Jilin-1 and socio-economic data. (a – c) Jilin-1 data sampled using irregular socio-economic polygons P1 and P2 labelled in (a). (d – f) Jilin-1 data sampled using a regular 100 m square grid falling within socio-economic polygons that were dissolved by class ID (merging neighbouring polygons with the same class). In this example, P1 and P2 were dissolved. Samples used all Jilin-1 data (a and d), data masked to WSF-2019 built up areas (b and e), or data masked to OpenStreetMap roads with a 10 m (each side) buffer (c and f).

2.4. Socio-economic analysis

We used socio-economic classification data (CIUQ 2020; Instituto Geográfico Militar 2019) to evaluate the spatial differences in night-time lighting. The dataset characterizes housing characteristics, education level, household economic activity, ownership of assets, access to technology, and consumption habits into five socio-economic classes, ranging from *High* to *Low*. These data also included a population projection (from the 2010 census) for year 2019. We sampled the night-time light data using two methods since the irregular socio-economic polygons had variable proportions of built-up areas and populations (Table S2). First, using the original irregular socio-economic polygons (Figure 4a-c), and second using a standardized 100 m square grid within the socio-economic polygons (Figure 4d-f). For each of these two methods, we sampled either all the intersecting night-time data (e.g. Figure 4a,d), data masked to the World Settlement Footprint 2019 (WSF-2019) built-up area mask (Marconcini et al. 2021) (e.g. Figure 4b,e), and data masked to a 10 m (radius) buffer of the OSM road network (e.g. Figure 4c,f). We exclude the following classes from the OSM road dataset for all analysis: steps, bridleway, cycleway, footway, raceway, track, construction, path, platform, bus stop, and pedestrian.

2.5. Other datasets

The World Settlement Footprint Evolution (WSF-Evo) (Marconcini et al. 2021) dataset documented global built-up area expansion 1985–2015 and was intersected with our light-type classification to identify potential trends in LED uptake through time. One limitation of this approach is that the WSF-Evo does not account for urban redevelopment with a city (e.g. Watson et al. 2022), therefore old areas of the city that were modernized with LED lighting would still feature the date of original urbanization.

A land cover classification we applied to a 13-band Sentinel-2 L1-C image (5th July 2021) at 10 m resolution (resampled where required) was also used to evaluate spatial trends in illumination classified into CORINE 2018 schema land cover classes. The classification used a pre-trained U-net deep learning model with a reported overall accuracy of 82% (Esri 2021). Additionally, we evaluated a dataset of green spaces including city parks and recreation grounds (CIUQ 2017) against the JL1-mean night-time data to quantify their degree of illumination.

3. Results

3.1. Georeferencing and image overlap

Orthorectification errors for the JL1-NT data ranged from 5.8 to 8.4 m CE95 (Table 1), whereas the OSM road-based georeferencing method featured errors over 300 m in areas of steep topography (Figure S1). Therefore, the orthorectified JL1-NT data were used for all further analysis, and the three images were merged into a city-wide image (Figure 5). Since the orthorectification errors restrict pixel-level comparisons, we compared the mean radiance values in the area of JL1-NT acquisition overlap at grid sizes of 50, 100, and 200 m, which revealed a trade-off between a reduction in root mean square error (RMSE) and sample size with an increasing grid size (Figure 6). A 100 m sample grid provided a suitable balance to sample spatial trends within socio-economic polygons whilst reducing RMSE, which ranged from 75 to 143 nanoWatts/cm²/sr for the two overlapping areas (Figure 6b, c). An example of the difference in radiance for the largest overlapping area is shown in Figure 7. There were notable differences in brightness between the overlapping JL1-NT acquisitions in flat areas of open green space, in built-up areas with a road network of varying orientation, and in areas of high-rise buildings (Figure 7).

3.2. Light type and street light classification

From the random forest light source classification, the precision, recall, and F1-scores for the LED class were 0.83, 0.66, and 0.74, respectively, whereas the same values for the HPS class were 0.72, 0.86, and 0.78. Therefore, the HPS classification was slightly more accurate. HPS was the main lighting type in Quito accounting for 74% (32.8 km²) of the observed illumination compared to 11.4 km² for LED sources (Figure 8). LED sources were distributed around the city with a core area of high-density LED in the historic centre (Figure 8c). LED sources were generally distinguishable by eye in the true-colour JL1-NT imagery (white and blues, Figure 8b, c, d), and the mean band radiance for the ground truth lights showed LED sources were overall brighter, especially in the blue band (Figure 9a).

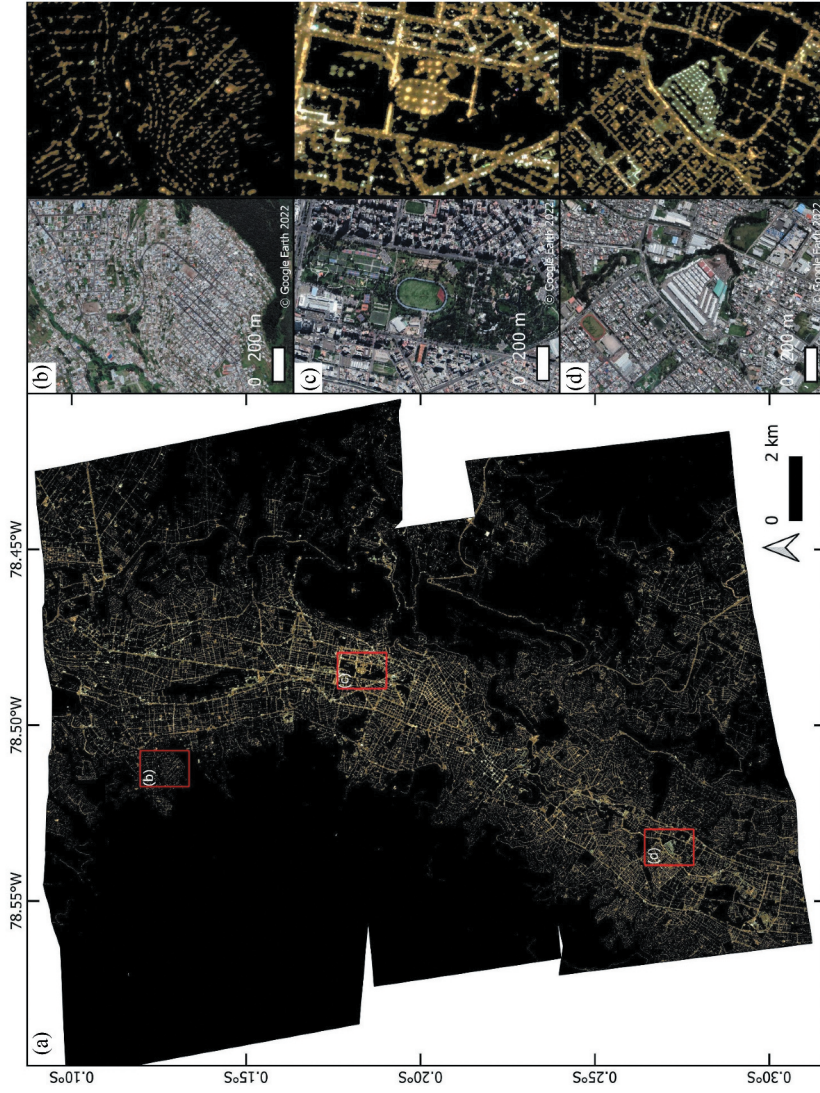


Figure 5. Overview of the Quito night-time imagery. (a) Orthorectified night-time imagery. (b) Atacucho neighbourhood shown in Google Satellite basemap imagery (left) and night-time image (right)(latitude: 0.12549°S, longitude: 78.51294°W). (c) La Carolina park (latitude: 0.18316°S, longitude: 78.48447°W). (d) Municipal Wholesale Market (centre of image) surrounded by residential development (latitude: 0.27144°S, longitude: 78.53409°W).

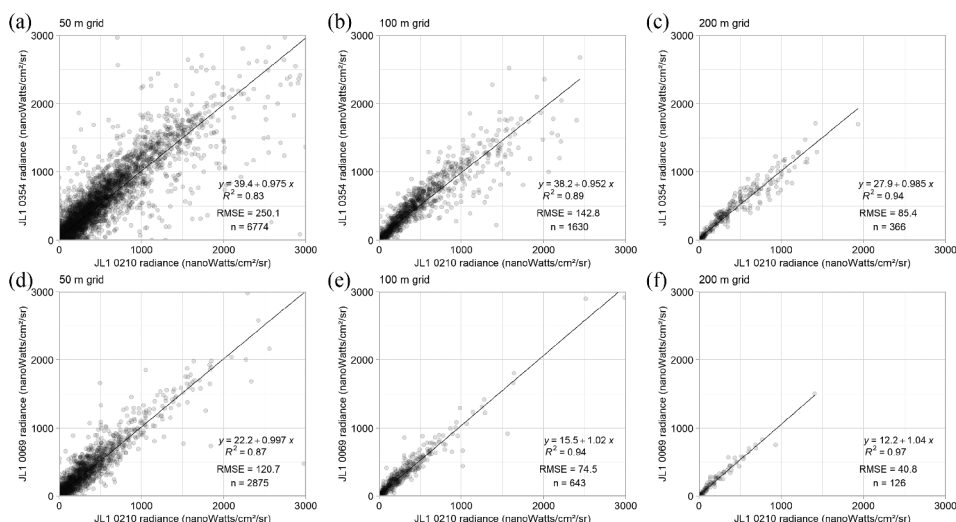


Figure 6. Plots of radiance for two areas of overlapping Jilin-1 images. (a – c) Overlapping images 0210 and 0354 (Table 1). (d – f) Overlapping images 0210 and 069. Mean radiance values were extracted on a regular grid of sizes 50 m (a and d), 100 m (b and e) and 200 m (c and f).

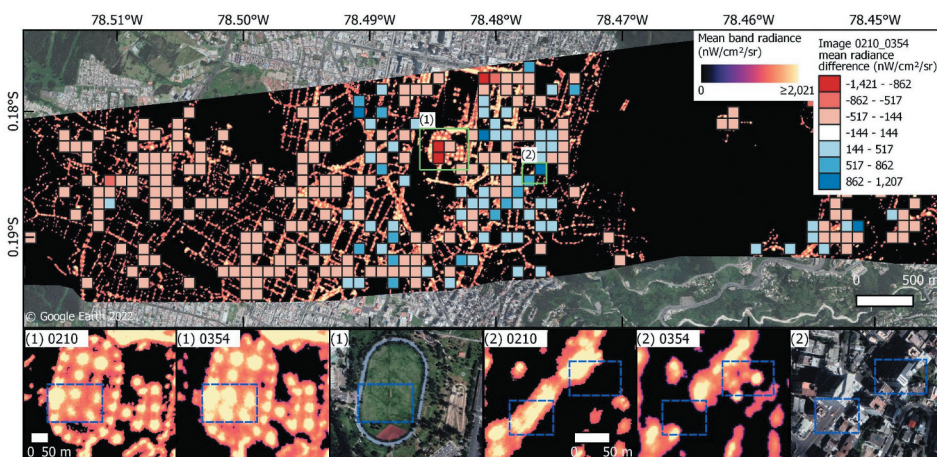


Figure 7. Example of Jilin-1 image overlap for images 0210 and 0354. Mean radiance values and the difference in mean radiance values between the two images are shown on a 100 m grid. Reds indicate areas where image 0354 had higher radiance values compared to image 0210, and blues indicate the opposite. Values ± 144 nanoWatts/cm²/sr (one standard deviation from the mean) are masked out for clarity. Insets for areas (1) and (2) show examples of the radiance values for an area of open green space and an area of high-rise buildings respectively.

Regarding the street light location classification, the F1-score was 0.71 with balanced omissions and commissions each totalling $\sim 29\%$ ($n = 186$) of the intersecting validation dataset ($n = 642$). A total of 90,279 street lights were classified and assigned source type, of which HPS made up 79% of the total number of lights and LED 21% (Table 2). The mean location difference between the classified and manually

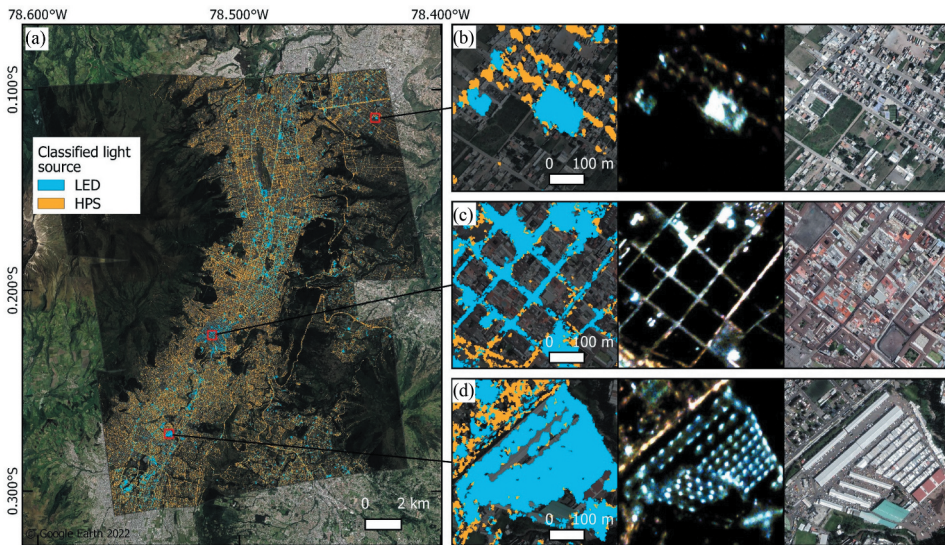


Figure 8. (a) LED and HPS light source classification. (b – d) Classification examples from each of the JL1 image acquisitions covering the north (b), centre (c) and south (d) of Quito. Panels (left to right) for (b – d) show the LED and HPS classification, the true colour JL1 image, and the Google Satellite Basemap view.

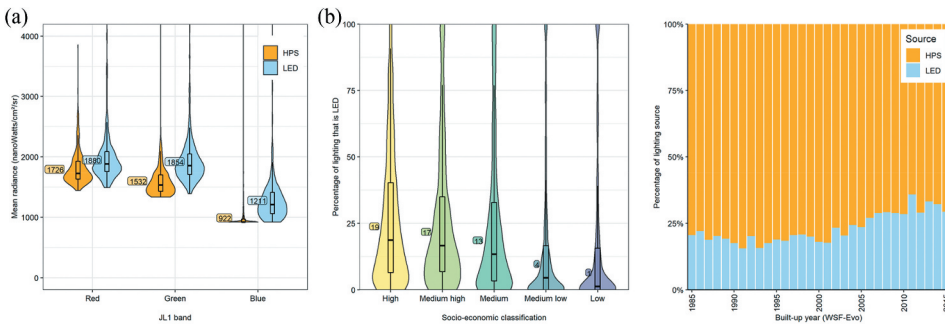


Figure 9. (a) Mean band radiance for the ground truth HPS and LED light sources. (b) Percentage of LED lighting by socio-economic classification. (c) Percentage HPS and LED lighting by built-up classification year from WSF-Evo, noting that this does not account for redevelopment, for example, the retrofitting of LED lighting in earlier built-up time periods (Section 2.5).

Table 2. Lighting type (high-pressure sodium and light emitting diode) and street light classification.

Light type	Classified area (km ²)	Classified street light count
HPS	11.4	71,140
LED	32.8	19,139
Total	44.2	90,279

mapped street lights was 3.8 ± 3.1 m. Examples of the street light classification are shown in Figure 10. Point sources of light were clearly identifiable when separated by decreasing illumination (Figure 10a, b), whereas localizing LED sources in the

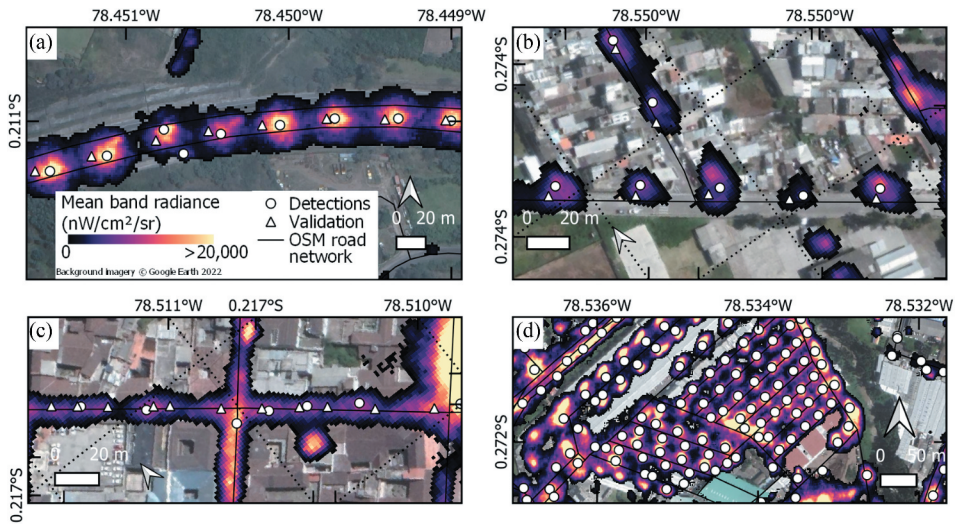


Figure 10. Examples of the street light location classification shown with the validation locations (a – c) and the JL1 mean band radiance used for the location classification. (d) Light classification in an area of LED lighting at the Municipal Wholesale Market corresponding to Figure 8d.

built-up areas was still possible but with higher emissions, since the illuminated coverage was greater and the light source spacing was smaller (e.g. Figure 10c). Notably, the mean and standard deviation street light spacing in the training data was 31.3 ± 10.2 m for HPS sources and 10.4 ± 4.1 m for LEDs. The latter were confined to the historic centre in the manually mapped street lights (Figure S2).

3.3. Spatial trends

3.3.1. Lighting type

The percentage of lighting that was from an LED source was smaller in the *Medium low* (4%) and *Low* (1%) socio-economic classifications compared to *High* (19%) and *Medium high* (17%) (Figure 9b). A trend in LED lighting through time was less apparent since LED sources were present in all built-up areas 1985–2015; however, the proportion of LED lighting increased to over 25% in the last 10 years (Figure 9c). Additionally, LED lighting was the most prevalent (39%) in the *Industrial commercial and transport unit* land cover class, which also featured the highest radiance (median = 443 nanoWatts/cm²/sr) (Figure 11). The *Urban fabric* class comprised 11% LED with a median radiance of 313 nanoWatts/cm²/sr (Figure 11). Other classes contained little illumination.

3.3.2. Illumination

The OSM road network was the dominant source of illumination across the AOI accounting for 45% of the illuminated pixels (brightness greater than zero) (Figure 12a). Built-up areas (WSF-2019) accounted for 23% of the total illumination and a 10 m buffer area between the road network and built-up areas also accounted for 23%, meaning that 68% of all illuminated pixels were on or within 10 m of a road. The total length and illuminated proportion of the road network was lowest for the *Medium low* and *Low* socio-economic

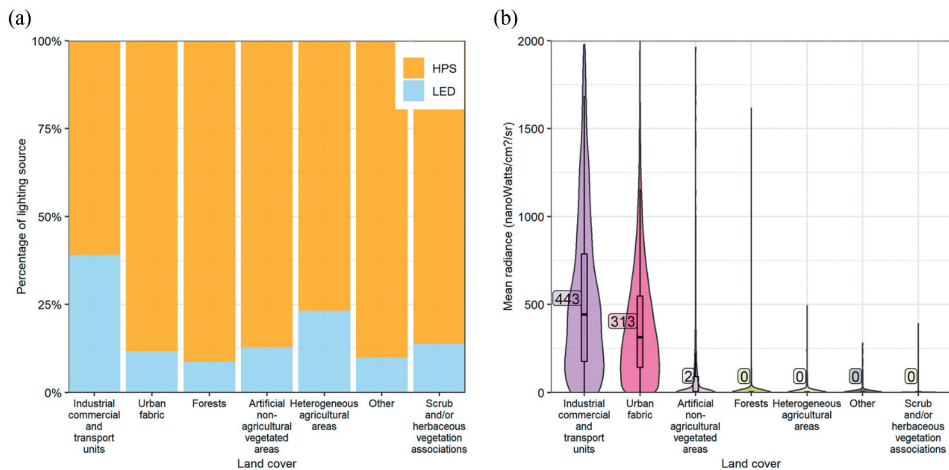


Figure 11. (a) Proportion of HPS and LED lighting in each land cover class for a Sentinel-2 land cover classification following the CORINE 2018 classification scheme. (b) Mean radiance values for each land cover class. Classes representing less than 5% of the total AOI are grouped into ‘Other’.

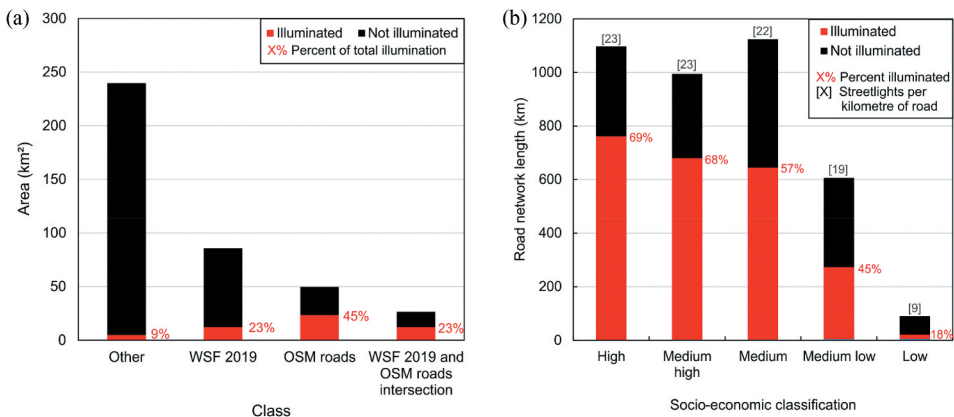


Figure 12. (a) Illumination attributed to mutually exclusive classes: built-up areas (WSF 2019), the road network (OSM roads), a transitional 10 m buffer between the road network and built-up areas (WSF 2019 and OSM roads intersection), and other undesignated areas (Other). (b) Illuminated road network and street lights per kilometre of road.

classes, in addition to the number of street lights per kilometre of road (Figure 12b). These two classes had 19 and 9 street lights per kilometre of road, respectively, compared to 23 for the *High* and *Medium high* classes.

Radiance values reduced with decreasing socio-economic classification for the two sampling methods (polygon and gridded (Figure 4)) and for each of the sampling areas (all JL1-NT data, built-up areas, and a 10 m road buffer) (Figure 13). The 10 m road buffer had the highest radiance values across all classes with median values of 722–948 nanoWatts/cm²/sr for the *High* and *Medium high* classes compared to 0–525 nanoWatts/cm²/sr for the *Low* and *Medium low* classes (Figure 13c,d). In comparison,

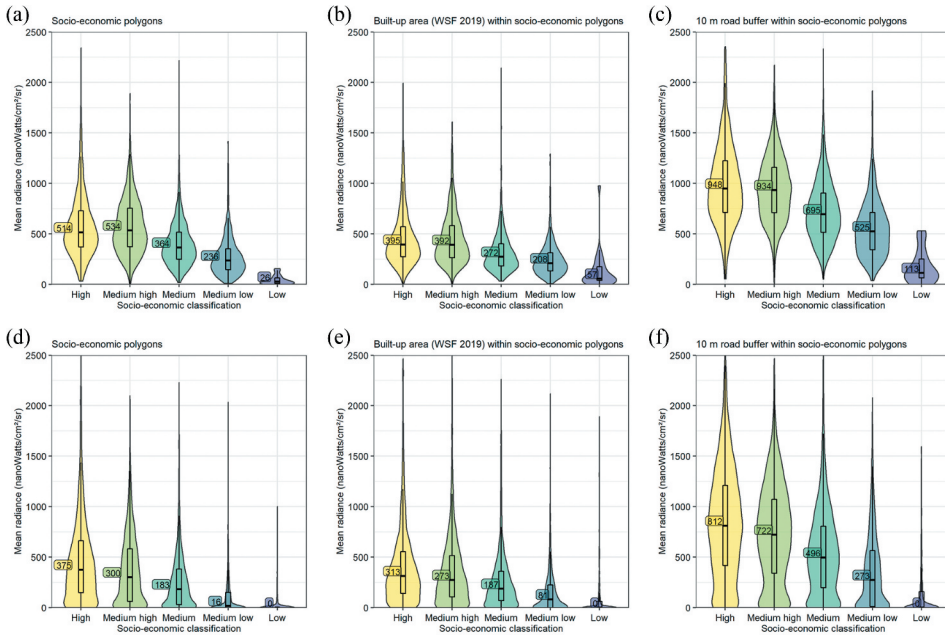


Figure 13. Mean radiance values within socio-economic classifications. (a – c) Mean radiance values sampled by individual socio-economic polygons (e.g. Fig 3 a – c). (d – f) mean radiance values sampled with a regular 100 m square grid falling within socio-economic polygons dissolved by class (e.g. Fig 3 d – f). The plots are derived using all Jilin-1 data (a and d), data masked to WSF-2019 built up areas (b and e), and data masked to OpenStreetMap roads with a 10 m (each side) buffer (c and f). Mann-Whitney U tests showed that there was a significant difference ($p < 0.5$) between the radiance in the High and Medium high groups compared to the Medium low and Low groups for (a – f).

the built-up areas had corresponding values of 273–395 (*High* and *Medium high*) and 0–208 (*Low* and *Medium low*) nanoWatts/cm²/sr respectively (Figure 13b,e).

Designated green space areas showed a similar illumination trend across socio-economic classes, with medium and higher classes having the greatest area of designated green space and with greatest illumination (Figure 14). Across all designated green spaces, the median percentage of illuminated area (brightness greater than zero) was 25% and 32% for *High* and *Medium high* classes compared to 6% and 0% for the *Medium low* and *Low* classes, respectively (Figure 14b).

4. Discussion

4.1. Using JL1 night-time imagery

Image orthorectification was essential to fully utilize the high-resolution JL1-NT data in the complex topography of Quito, especially when comparing multiple acquisitions since the light sources and illumination patterns are more dynamic than an equivalent optical satellite image for example (Levin et al. 2020). Positional accuracy of our JL1-NT data ranged from 5.8 to 8.4 m CE95 (Table 1) following orthorectification. One other study reported JL1-NT image georeferencing errors, which ranged from 52 to 63 m using spline transformations (Guk and Levin 2020). The lack of reporting of the image processing level

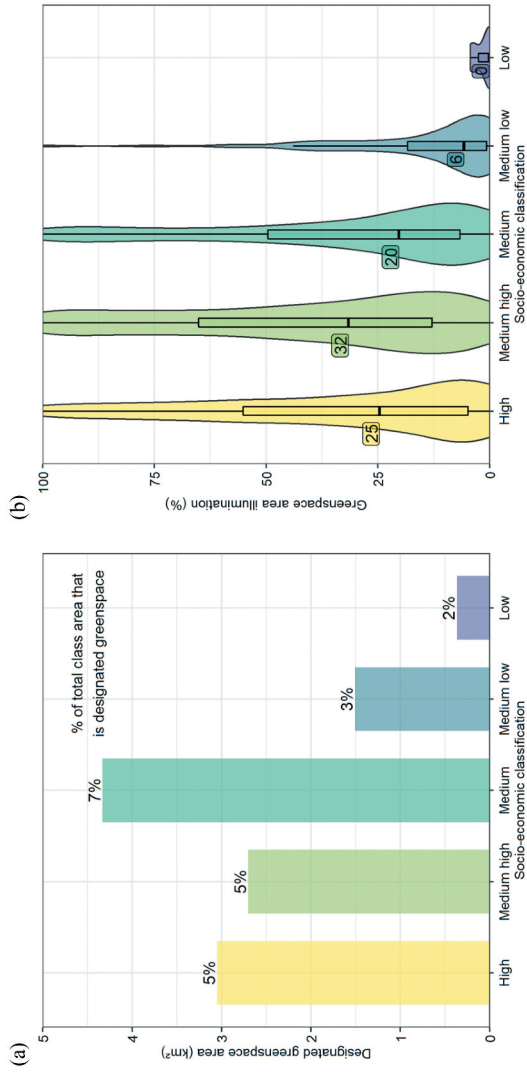


Figure 14. (a) Green space area and proportional coverage for areas of each socio-economic class. (b) Percentage of green space that is illuminated for all designated green spaces falling within socio-economic polygons.

(e.g. orthorectified or not) and georeferencing errors in other studies restricts comparisons. Nonetheless, Guk and Levin (2020) also compared the radiance in an overlapping area of two JL1-NT images and found improved correlations using coarser sampling grids. Their correlation coefficients (maximum 0.71) were smaller than what we observed (0.89–0.94) using the same grid size (100 m), potentially since their acquisitions were separated by 3 days with similar acquisition geometries, whereas ours were near simultaneous (within 2 min). Guk and Levin (2020) calculated illumination statistics on a 100 m grid, which we also used after evaluating the RMSE in two overlapping areas. The maximum RMSE we observed was 143 nanoWatts/cm²/sr (Figure 6b), which although notable, was smaller than the differences we evaluated with socio-economic and landcover datasets. Nonetheless, the differences in observed radiance in the overlapping areas highlight the importance of image acquisition geometry and preclude pixel-level comparisons (Figure 6, 7). The effects of screening and variable illumination sources and directions (e.g. Figure 1) also mean that the observed radiance is a function of local geometry that cannot be accounted for with a single correction (Levin et al. 2020), although a high-resolution DEM incorporating building heights and footprints could offer some insights.

4.2. Light type and street light classification

Several studies have used night-time imagery to classify light source types into HPS and LED classes. Zheng et al. (2018) used a workflow including ISODATA clustering, manual class merging, and a decision tree classifier, whereas Cheng et al. (2020) used a maximum likelihood classifier. We obtained a good classification accuracy (F1 = 0.72–0.83) using a shark random forest decision tree approach, which had the benefit of computational simplicity and low sensitivity to training data noise since our light types were not validated in the field. Our street light classification had an F1-score of 0.71 with balanced omissions and commissions. Intersecting the street light classification with the light type classification revealed a breakdown of 79% ($n = 71,140$) HPS lights and 21% ($n = 19,139$) LED (Table 2). Independent validation datasets were not available, though the electric utility company Empresa Eléctrica Quito reported a breakdown of 92.3% ($n = 260,949$) HPS, 1.7% ($n = 4,738$) LED and 6% other public light sources for a $> 13,000$ km² area incorporating our study area (401 km²) (Galindo, Borge-Diez, and Icaza 2022; ARCONEL 2020). Therefore, our study reported a higher number of LED sources despite covering a much smaller area. This could be due in part to incorrect light type assignment in areas where LED sources dominate from buildings, rather than street lights, though is potentially due to the inclusion of non-public lighting sources, which we could not distinguish from public sources. This is supported by our ground truth dataset of 200 LED street lights in a small area of Quito's historic centre covering 2 km of road. This area had over 45 km of LED-lit streets (e.g. Figure 8a, c) and could therefore potentially account for over 4,300 LED lights based on our observed 10.4 m mean spacing.

Lighting type is an indicator of infrastructure modernization as HPS sources are replaced with energy-efficient LEDs (Pimputkar et al. 2009; Bachanek et al. 2021) (Figure 9b). We demonstrated that JL1-NT data provided valuable mapping capabilities able to classify and locate street lights; however, the georeferencing uncertainties we observed in complex topography (5.8–8.4 m CE95 (Table 1)) may hinder multi-temporal

automated monitoring of specific light sources, especially when radiometric calibration and atmospheric corrections are not applied (Levin et al. 2020). Nonetheless, the relative low cost of the JL1-NT imagery (~\$2,500 for our study area) should enable repeat acquisitions to monitor changes and improve calibration through time.

4.3. Illumination characteristics

4.3.1. Socio-economic trends

The association between illumination and socio-economic census data that we observed across Quito demonstrated that valuable information on inequalities in lighting distribution can be quantified using JL1-NT data at a city level. This was expected since similar trends were observed using coarse resolution night-time imagery (Henderson, Storeygard, and Weil 2011; Elvidge et al. 2012), though demonstrates the potential for more detailed evaluation of smaller areas, such as informal settlements. The relationship between lighting distribution and informal settlements in the case of Quito is important, as access to this service, like others such as water and sewerage, is universal. This implies that informal settlements have the right to request electric lighting services, even if they are not part of the city's territorial planning. However, in reality, universal access has limitations related to the management capacity of Empresa Eléctrica Quito, which is in charge of providing the service. Our study was able to evaluate the difference in the level of lighting present in the different socio-economic sectors. In the higher socio-economic classes, we observed higher proportions of LED lighting (Figure 9b), higher proportions of road network lighting and density of street lights (Figure 12b), higher mean radiance for built-up areas and the road network (Figure 13), and greater coverage and illumination of designated green spaces (Figure 14). The *High* and *Medium high* classes accounted for a total population of 915,900 people compared to 121,200 for the *Medium low* and *Low* classes (Table S2) although we did not observe a relationship between population and illumination (Figure S3).

The spatial characteristics of the city, such as its topography, layout, and morphology, influence the structural conditions of socio-economic inequality, which in turn affect levels of insecurity (SSG., Secretaría de Seguridad y Gobernabilidad 2021). This spatial reality is in turn reflected in the lighting levels of public space and helps to understand the link between lower street lighting coverage and higher levels of socio-economic vulnerability (Figure 12b), especially in peripheries and areas of informal expansion (Interview AC2). The specific causes and consequences of these trends were not evaluated in this study, though studies have shown, for example that light accessibility promotes economic activity, including the extension of trading hours (Karekezi and Majoro 2002; Bouman 1987), and that lighting is associated with reduced social disorder and improved perception of safety and was therefore historically more abundant in affluent areas (Moran et al. 2022; Clarke 2008; Bouman 1987). However, the potential negative effects of ALAN on public health and nature (Keshet-Sitton et al. 2017; Navara and Nelson 2007; Hölker et al. 2010) mean that addressing lighting inequalities is a complex issue.

4.3.2. Perceptions of security

Night-time images could be used where violence and the perception of insecurity are of concern to citizens (SSG., Secretaría de Seguridad y Gobernabilidad 2021) since this is related to a lack of lighting in streets and public spaces. This influences the use of certain sectors of cities such as Quito, both spatially (avoiding places with poor lighting) and temporally (restriction of walking at night). Some statistics suggest that nine out of ten citizens feel unsafe in Quito (Interview E 2023); eight out of ten say they have changed their habits for fear of some kind of crime (SSG., Secretaría de Seguridad y Gobernabilidad 2021); and seven out of ten feel higher levels of insecurity at night (Tapia 2022). Therefore, the demand for public lighting in various sectors of Quito is related to security strategies aimed at reducing the perception of fear, encouraging the use and appropriation of public spaces, and to dissuade delinquency (Interview E 2023).

In Quito, the demands for lighting are channelled to the municipality through the neighbourhood safety committees. First, a diagnosis of the hotspots of insecurity is carried out in the territory; subsequently, the Secretaria de Seguridad Ciudadana y Gobernabilidad makes agreements with Empresa Eléctrica Quito, which grants a number of lighting quotas for the sites prioritized by the community (Interview E 2023, 2023, 2023). However, in some parts of the city, the lighting of public spaces has had adverse effects, such as problems of coexistence related to increased alcohol consumption in these areas (Interview E 2023).

4.4. Future applications

The high-resolution of JL1-NT enables analysis at a community level, even when degrading the analysis to a 100 m grid to reduce uncertainties. Therefore, the broad applications of night-time imagery (Figure 1) make it relevant for addressing a range of SDGs (Stokes and Seto 2019; Ivan et al. 2020), especially to provide proxy information on development and electrification status in data-poor areas. Urban areas are projected to continue to expand in coming decades (Chen et al. 2020; Jing and O'Neill 2020). Therefore, future urban growth presents an opportunity to modify the spatio-temporal dynamics of ALAN to minimize negative social, environmental, and ecological effects (Gaston et al. 2012). Our methodology using JL1-NT imagery is transferable to other locations since we used open access datasets with near global coverage to process the data (e.g. the GLO-30 DEM) and evaluate spatial trends, including the OSM Road network, light source validation data from Google Earth and Google Street View, a land cover classification derived using Sentinel-2 imagery, a built-up area mask from the WSF-2019 dataset, and an urban growth classification obtained from the WSF-Evo dataset.

In the case of cities such as Quito, ALAN could become an input to environmental, climate action, productive development, and public safety plans. For example, the Plan Metropolitano de Ordenamiento Territorial (PMDOT) sees street lighting primarily as an infrastructure problem and ALAN is indirectly addressed in the public space management and mobility plans (Municipio del Distrito Metropolitano de Quito – MDMQ 2021). In terms of urban design, for example, since 2014, Empresa Eléctrica Quito and the Instituto Metropolitano de Patrimonio, have promoted a lighting project in the city's historic

centre, in streets, squares and churches, based on aesthetic criteria (enhancement of architectural heritage) and energy efficiency (use of LED technology) (e.g. [Figure 8c](#)). JL1-NT imagery offers city planners a unique tool with the capability to identify individual light sources such as street lights, buildings, and recreational spaces. However, since the JL1-NT acquisition is for a single point in time, the notable spatial and temporal variation in urban lighting cannot be captured. These changes can instead be characterized using uncrewed aerial vehicle surveys, although these cover smaller areas and are time intensive (Li et al. 2020).

5. Conclusion

In this study, we evaluated the applications of night-time satellite imagery over the expanding and topographically complex city of Quito, Ecuador. We orthorectified three ~1.5 m resolution multi-spectral night-time acquisitions from the Jilin-1 Gaofen-03C01 satellite with an accuracy (5.8–8.4 m CE95). We then developed a classification to distinguish high-pressure sodium and light emitting diode sources (F1-score = 0.72–0.83) using a shark random forest decision tree approach. We found that the road network was the dominant source of illumination, accounting for 45% of illuminated pixels (68% of all illuminated pixels were on or within 10 m of a road), whereas built-up areas accounted for 23%. Additionally, higher socio-economic development was associated with higher proportions of LED lighting, greater road network lighting and density of street lights, higher overall radiance in built-up areas, and greater illumination of designated green spaces. Our analysis highlighted the ability of Jilin-1 night-time satellite imagery to map and monitor light sources at high-resolution. However, image acquisition geometry, local topography, and built-up areas affects the observed radiance and would require consideration when evaluating spatial and temporal trends within and between study locations.

Acknowledgements

This research has been supported by a NERC Innovation award (NE/S013911/1), the UK Research and Innovation (UKRI) Global Challenges Research Fund (GCRF) Urban Disaster Risk Hub (NE/S009000/1) (Tomorrow's Cities), and COMET. COMET is the NERC Centre for the Observation and Modelling of Earthquakes, Volcanoes and Tectonics, a partnership between UK Universities and the British Geological Survey. John Elliott is supported by a Royal Society University Research fellowship (UF150282).

Disclosure statement

No potential conflict of interest was reported by the authors.

Funding

The work was supported by the Natural Environment Research Council [NE/S013911/1]; UK Research and Innovation Global Challenges Research Fund [NE/S009000/1]

ORCID

C. Scott Watson  <http://orcid.org/0000-0003-2656-961X>

Santiago Bonilla-Bedoya  <http://orcid.org/0000-0002-2464-4500>

Data availability statement

Datasets supporting this study are available in the Zenodo repository: <https://doi.org/10.5281/zenodo.7695019>

References

- Airbus Defence and Space GmbH. 2020. "Copernicus DEM -Copernicus Digital Elevation Model Product Handbook. Accessed 16th December 2022. Available from:https://object.cloud.sdsc.edu/v1/AUTH_opentopography/www/metadata/Copernicus_metadata.pdf."
- ARCONEL. 2020. "Agencia de Regulación y Control de la Electricidad, Estadística Anual y Multianual Sector Eléctrico Ecuatoriano 2019 Año 2020. Available from: https://www.regulacionelectricagob.ec/wp-content/uploads/downloads/2020/06/Est_2019_Borrador_08-06-2020_1606.pdf. Accessed 21th December 2022."
- Bachanek, K. H., B. Tundys, T. Wiśniewski, E. Puzio, and A. Maroušková. 2021. "Intelligent Street Lighting in a Smart City Concepts—A Direction to Energy Saving in Cities: An Overview and Case Study." *Energies* 14 (11): 3018. doi:10.3390/en14113018.
- Bonilla-Bedoya, S., A. Mora, A. Vaca, A. Estrella, and M. Ángel Herrera. 2020. "Modelling the Relationship Between Urban Expansion Processes and Urban Forest Characteristics: An Application to the Metropolitan District of Quito." *Computers, Environment and Urban Systems* 79: 101420. doi:10.1016/j.compenvurbsys.2019.101420.
- Bouman, M. J. 1987. "Luxury and Control: The Urbanity of Street Lighting in Nineteenth-Century Cities." *Journal of Urban History* 14 (1): 7–37. doi:10.1177/009614428701400102.
- Bruederle, A., and R. Hodler. 2018. "Nighttime Lights as a Proxy for Human Development at the Local Level." *PloS One* 13 (9): e0202231. doi:10.1371/journal.pone.0202231.
- Chatelain, J. L., B. Tucker, B. Guillier, F. Kaneko, H. Yepes, J. Fernandez, J. Valverde, et al. 1999. "Earthquake Risk Management Pilot Project in Quito, Ecuador." *GeoJournal* 49 (2): 185–196. doi:10.1023/A:1007079403225.
- Cheng, B., Z. Chen, B. Yu, Q. Li, C. Wang, B. Li, B. Wu, Y. Li, and J. Wu. 2020. "Automated Extraction of Street Lights from JL1-3B Nighttime Light Data and Assessment of Their Solar Energy Potential." *IEEE Journal of Selected Topics in Applied Earth Observations and Remote Sensing* 13: 675–684. doi:10.1109/JSTARS.2020.2971266.
- Chen, G., L. Xia, X. Liu, Y. Chen, X. Liang, J. Leng, X. Xiaocong, et al. 2020. "Global Projections of Future Urban Land Expansion Under Shared Socioeconomic Pathways." *Nature Communications* 11 (1): 537. doi:10.1038/s41467-020-14386-x.
- CIUQ. 2017. "Areas_verdes [Online]. [Accessed 19 December 2022]. Available from: <https://www.ciuq.ec/descargas/descargas.html>
- CIUQ. 2020. "Nivel_socioeconomico_2019 [online]. [Accessed 19 December 2022]. Available from: <https://www.ciuq.ec/descargas/descargas.html>
- Clarke, R. V. G. 2008. *Improving Street Lighting to Reduce Crime in Residential Areas*. Washington, DC, USA: US Department of Justice, Office of Community Oriented Policing Services.
- Contributors, O. 2022. OpenStreetMap. [online]. Accessed 17 November 2022. Available from: <https://www.openstreetmap.org>.
- Davies, T. W., and T. Smyth. 2018. "Why Artificial Light at Night Should Be a Focus for Global Change Research in the 21st Century." *Global Change Biology* 24 (3): 872–882. doi:10.1111/gcb.13927.

- Doll Christopher, N. H., J.P. Muller, and C. D. Elvidge. 2000. "Night-Time Imagery as a Tool for Global Mapping of Socioeconomic Parameters and Greenhouse Gas Emissions." *AMBIO: A Journal of the Human Environment* 29 (3): 157–626. doi:10.1579/0044-7447-29.3.157.
- EDAP. 2022. "Technical-Note-On-Quality-Assessment-For-Jilin-1-SP-And-GF03C-Video. Accessed 16th December 2022. Available from:https://www.google.com/url?sa=t&rct=j&q=&esrc=s&source=web&cd=&ved=2ahUKEwjrvZf0r_77AhWOiFwKHYJgAT4QFnoECBMQAQ&url=https%3A%2F%2Fearth.esa.int%2Fgateway%2Fdocuments%2F20142%2F37627%2FTechnical-Note-on-Quality-Assessment-for-Jilin-1-SP-and-GF03C-Video&usg=AOvVaw2YDYoy6KSHZqygyFQX9x."
- Elvidge, C. D., K. E. Baugh, S. J. Anderson, P. C. Sutton, and T. Ghosh. 2012. "The Night Light Development Index (NLDI): A Spatially Explicit Measure of Human Development from Satellite Data." *Social Geography* 7 (1): 23–35. doi:10.5194/sg-7-23-2012.
- Esri. 2021. "Land Cover Classification (Sentinel-2). [online]. Accessed 25 August 2021. Available from: <https://www.arcgis.com/home/item.html?id=afd124844ba84da69c2c533d4af10a58>
- French, E. L., S. Jeff Birchall, K. Landman, and R. D. Brown. 2019. "Designing Public Open Space to Support Seismic Resilience: A Systematic Review." *International Journal of Disaster Risk Reduction* 34: 1–10. doi:10.1016/j.ijdrr.2018.11.001.
- Galindo, S. P., D. Borge-Diez, and D. Icaza. 2022. "Energy Sector in Ecuador for Public Lighting: Current Status." *Energy Policy* 160: 112684. doi:10.1016/j.enpol.2021.112684.
- Gaston, K. J., T. W. Davies, J. Bennie, J. Hopkins, and E. Fernandez-juricic. 2012. "REVIEW: Reducing the Ecological Consequences of Night-Time Light Pollution: Options and Developments." *The Journal of Applied Ecology* 49 (6): 1256–1266. doi:10.1111/j.1365-2664.2012.02212.x.
- Giacomo, F., S. Pachauri, E. Byers, O. Danylo, and S. C. Parkinson. 2020. "Satellite Observations Reveal Inequalities in the Progress and Effectiveness of Recent Electrification in Sub-Saharan Africa." *One Earth* 2 (4): 364–379. doi:10.1016/j.oneear.2020.03.007.
- Giavi, S., S. Blösch, G. Schuster, and E. Knop. 2020. "Artificial Light at Night Can Modify Ecosystem Functioning Beyond the Lit Area." *Scientific Reports* 10 (1): 11870. doi:10.1038/s41598-020-68667-y.
- Guk, E., and N. Levin. 2020. "Analyzing Spatial Variability in Night-Time Lights Using a High Spatial Resolution Color Jilin-1 Image – Jerusalem as a Case Study." *ISPRS Journal of Photogrammetry and Remote Sensing* 163: 121–136. doi:10.1016/j.isprsjprs.2020.02.016.
- Hall, M. L., P. Samaniego, J. L. Le Pennec, and J. B. Johnson. 2008. "Ecuadorian Andes Volcanism: A Review of Late Pliocene to Present Activity." *Journal of Volcanology and Geothermal Research* 176 (1): 1–6. doi:10.1016/j.jvolgeores.2008.06.012.
- Henderson, V., A. Storeygard, and D. N. Weil. 2011. "A Bright Idea for Measuring Economic Growth." *The American Economic Review* 101 (3): 194–199. doi:10.1257/aer.101.3.194.
- Hölker, F., C. Wolter, E. K. Perkin, and K. Tockner. 2010. "Light Pollution as a Biodiversity Threat." *Trends in Ecology & Evolution* 25 (12): 681–682. doi:10.1016/j.tree.2010.09.007.
- Instituto Geográfico Militar. 2019. *Generation of Geospatial Information at a Scale 1: 5 000 for the Determination of the Physical Fitness of the Territory and Urban Development Through the Use of Geotechnologies [Spanish]*. Quito, Ecuador: Instituto Geográfico Militar.
- Interview E1. 2023. "Interview E1, F, L. Interviewer: Jonathan Menoscal. 7/02/2023. Unidad de Seguridad ciudadana."
- Interview E2. 2023. "Interview E2, T, J. Interviewer: Jonathan Menoscal. 7/02/2023. Secretaría de Seguridad y Gobernabilidad."
- Interview E3. 2023. "Interview E3, C, C. Interviewer: Jonathan Menoscal. 7/02/2023. Empresa Eléctrica Quito."
- Ivan, K., I.H. Holobăcă, J. Benedek, and I. Török. 2020. "Potential of Night-Time Lights to Measure Regional Inequality." *Remote Sensing* 12 (1): 33. doi:10.3390/rs12010033.
- Jing, G., and B. C. O'Neill. 2020. "Mapping Global Urban Land for the 21st Century with Data-Driven Simulations and Shared Socioeconomic Pathways." *Nature Communications* 11 (1): 2302. doi:10.1038/s41467-020-15788-7.
- Karekezi, S., and L. Majoro. 2002. "Improving Modern Energy Services for Africa's Urban Poor." *Energy Policy* 30 (11): 1015–1028. doi:10.1016/S0301-4215(02)00055-1.

- Katz, Y., and N. Levin. 2016. "Quantifying Urban Light Pollution — a Comparison Between Field Measurements and EROS-B Imagery." *Remote Sensing of Environment* 177: 65–77. doi:10.1016/j.rse.2016.02.017.
- Keshet-Sitton, A., K. Or-Chen, E. Huber, and A. Haim. 2017. "Illuminating a Risk for Breast Cancer: A Preliminary Ecological Study on the Association Between Streetlight and Breast Cancer." *Integrative Cancer Therapies* 16 (4): 451–463. doi:10.1177/1534735416678983.
- León, J., and A. March. 2016. "An Urban Form Response to Disaster Vulnerability: Improving Tsunami Evacuation in Iquique, Chile." *Environment and Planning B, Planning & Design* 43 (5): 826–847. doi:10.1177/0265813515597229.
- Levin, N., C. C. M. Kyba, Q. Zhang, A. S. de Miguel, M. O. Román, X. Li, B. A. Portnov, et al. 2020. "Remote Sensing of Night Lights: A Review and an Outlook for the Future." *Remote Sensing of Environment* 237: 111443. doi:10.1016/j.rse.2019.111443.
- Li, X., N. Levin, J. Xie, and L. Deren. 2020. "Monitoring Hourly Night-Time Light by an Unmanned Aerial Vehicle and Its Implications to Satellite Remote Sensing." *Remote Sensing of Environment* 247: 111942. doi:10.1016/j.rse.2020.111942.
- Lloyd, C. T., A. Sorichetta, and A. J. Tatem. 2017. "High Resolution Global Gridded Data for Use in Population Studies." *Scientific Data* 4 (1). doi:10.1038/sdata.2017.1.
- Loewen, L. J., G. Daniel Steel, and P. Suedfeld. 1993. "Perceived Safety from Crime in the Urban Environment." *Journal of Environmental Psychology* 13 (4): 323–331. doi:10.1016/S0272-4944(05)80254-3.
- Marconcini, M., N. Gorelick, A. Metz-Marconcini, and T. Esch. 2020. "Accurately Monitoring Urbanization at Global Scale – the World Settlement Footprint." *IOP Conference Series: Earth and Environmental Science* 509 (1): 012036. doi:10.1088/1755-1315/509/1/012036.
- Marconcini, M., A. Metz-Marconcini, T. Esch, and N. Gorelick. 2021. *Understanding Current Trends in Global Urbanisation-The World Settlement Footprint Suite*. doi:10.1553/giscience2021_01_s33.
- Mellander, C., J. Lobo, K. Stolarick, and Z. Matheson. 2015. "Night-Time Light Data: A Good Proxy Measure for Economic Activity?" *PloS One* 10 (10): e0139779. doi:10.1371/journal.pone.0139779.
- Min, B., and K. Mensan Gaba. 2014. "Tracking Electrification in Vietnam Using Nighttime Lights." *Remote Sensing* 6 (10): 9511–9529. doi:10.3390/rs6109511.
- Molthan, A., and G. Jedlovac. 2013. "Satellite Observations Monitor Outages from Superstorm Sandy." *Eos, Transactions American Geophysical Union* 94 (5): 53–54. doi:10.1002/2013EO050001.
- Moran, M. R., D. A. Rodríguez, A. Cortinez-O’Ryan, and J. Jaime Miranda. 2022. "Is Self-Reported Park Proximity Associated with Perceived Social Disorder? Findings from Eleven Cities in Latin America." *Landscape and Urban Planning* 219: 104320. doi:10.1016/j.landurbplan.2021.104320.
- Municipio del Distrito Metropolitano de Quito – MDMQ. 2021. Plan Metropolitano de Desarrollo y Ordenamiento Territorial 2021-2033 [online]. Accessed 2nd February 2023. Available from: <https://gobiernoabierto.quito.gob.ec/plan-pmdot/>
- Navara, K. J., and R. J. Nelson. 2007. "The Dark Side of Light at Night: Physiological, Epidemiological, and Ecological Consequences." *Journal of Pineal Research* 43 (3): 215–224. doi:10.1111/j.1600-079X.2007.00473.x.
- Noam, L., K. Johansen, J. M. Hacker, and S. Phinn. 2014. "A New Source for High Spatial Resolution Night Time Images — the EROS-B Commercial Satellite." *Remote Sensing of Environment* 149: 1–12. doi:10.1016/j.rse.2014.03.019.
- Pawson, S. M., and M.K. -F. Bader. 2014. "LED Lighting Increases the Ecological Impact of Light Pollution Irrespective of Color Temperature." *Ecological Applications* 24 (7): 1561–1568. doi:10.1890/14-0468.1.
- Pedrosa, E. L. J., S. Asare Okyere, L. Kusi Frimpong, S. Kofi Diko, T. Sidney Commodore, and M. Kita. 2021. "Planning for Informal Urban Green Spaces in African Cities: Children’s Perception and Use in Peri-Urban Areas of Luanda, Angola." *Urban Science* 5 (3): 50. doi:10.3390/urbansci5030050.
- Peled, Y., and T. Fishman. 2021. "Estimation and Mapping of the Material Stocks of Buildings of Europe: A Novel Nighttime Lights-Based Approach." *Resources Conservation and Recycling* 169: 105509. doi:10.1016/j.resconrec.2021.105509.
- Pimputkar, S., J. S. Speck, S. P. DenBaars, and S. Nakamura. 2009. "Prospects for LED Lighting." *Nature Photonics* 3 (4): 180–182. doi:10.1038/nphoton.2009.32.

- Qiang, Y., Q. Huang, and X. Jinwen. 2020. "Observing Community Resilience from Space: Using Nighttime Lights to Model Economic Disturbance and Recovery Pattern in Natural Disaster." *Sustainable Cities and Society* 57: 102115. doi:10.1016/j.scs.2020.102115.
- Schwind, P., and T. Storch. 2022. "Georeferencing Urban Nighttime Lights Imagery Using Street Network Maps." *Remote Sensing* 14 (11): 2671. doi:10.3390/rs14112671.
- Shi, L., G. M. Foody, D. S. Boyd, R. Girindran, L. Wang, D. Yun, and F. Ling. 2020. "Night-Time Lights are More Strongly Related to Urban Building Volume Than to Urban Area." *Remote Sensing Letters* 11 (1): 29–36. doi:10.1080/2150704X.2019.1682709.
- Sierra, A. 2009. "La política de mitigación de los riesgos en las laderas de Quito: ¿qué vulnerabilidad combatir?" *Bulletin de l'Institut français d'études andines*, no. 38 (3): 737–753. doi:10.4000/bifea.2421.
- SSG., Secretaría de Seguridad y Gobernabilidad. 2021. *Plan Metropolitano de Seguridad Ciudadana y Convivencia Pacífica en el DMQ*. Quito, Ecuador: Municipio del Distrito Metropolitano de Quito.
- Steinbach, R., C. Perkins, L. Tompson, S. Johnson, B. Armstrong, J. Green, C. Grundy, P. Wilkinson, and P. Edwards. 2015. "The Effect of Reduced Street Lighting on Road Casualties and Crime in England and Wales: Controlled Interrupted Time Series Analysis." *Journal of Epidemiology and Community Health* 69 (11): 1118–1124. doi:10.1136/jech-2015-206012.
- Stokes, E. C., and K. C. Seto. 2019. "Characterizing Urban Infrastructural Transitions for the Sustainable Development Goals Using Multi-Temporal Land, Population, and Nighttime Light Data." *Remote Sensing of Environment* 234: 111430. doi:10.1016/j.rse.2019.111430.
- Stone, E. L., G. Jones, and S. Harris. 2012. "Conserving Energy at a Cost to Biodiversity? Impacts of LED Lighting on Bats." *Global Change Biology* 18 (8): 2458–2465. doi:10.1111/j.1365-2486.2012.02705.x.
- Sutton, P., D. Roberts, C. Elvidge, and K. Baugh. 2001. "Census from Heaven: An Estimate of the Global Human Population Using Night-Time Satellite Imagery." *International Journal of Remote Sensing* 22 (16): 3061–3076. doi:10.1080/01431160010007015.
- Tan, M., L. Xiubin, L. Shiji, L. Xin, X. Wang, L. Qian, L. Wei, L. Yuanyuan, and W. Xiang. 2018. "Modeling Population Density Based on Nighttime Light Images and Land Use Data in China." *Applied Geography* 90: 239–247. doi:10.1016/j.apgeog.2017.12.012.
- Tapia, R. 2022. La influencia de las estrategias preventivas en el miedo al crimen MAC: caso del Distrito Metropolitano de Quito 2014-2018. Tesis para obtener el título de maestría de investigación en Estudios Urbanos. Flacso, Ecuador. [online]. Accessed 2nd February 2023. Available from: <https://repositorio.flacsoandes.edu.ec/handle/10469/18185>
- Touitou, Y., A. Reinberg, and D. Touitou. 2017. "Association Between Light at Night, Melatonin Secretion, Sleep Deprivation, and the Internal Clock: Health Impacts and Mechanisms of Circadian Disruption." *Life Sciences* 173: 94–106. doi:10.1016/j.lfs.2017.02.008.
- Valcárcel, J. A., V. Despotaki, C. G. Burton, C. Yepes-Estrada, V. Silva, and C. Villacis. 2017. "Integrated Assessment of Earthquake Risk in Quito, Ecuador Using Openquake." Paper presented at the 16th World Conference on Earthquake Engineering, Santiago, Chile, 16WCEE.
- Vidal, X., L. Burgos, and O. Zevallos. 2015. "11 Protection and Environmental Restoration of the Slopes of Pichincha in Quito, Ecuador." *Water and Cities in Latin America: Challenges for Sustainable Development* 181–196.
- Wang, Z., M. O. Román, Q. Sun, A. L. Molthan, L. A. Schultz, and V. L. Kalb. 2018. "Monitoring Disaster-Related Power Outages Using NASA Black Marble Nighttime Light Product." *ISPRS International Archives of the Photogrammetry, Remote Sensing and Spatial Information Sciences* 2018: 1853–1856. doi:10.5194/isprs-archives-XLII-3-1853-2018.
- Watson, C. S., J. R. Elliott, R. M. J. Amey, and E. A. Kanatbek. 2022. "Analyzing Satellite-Derived 3D Building Inventories and Quantifying Urban Growth Towards Active Faults: A Case Study of Bishkek, Kyrgyzstan." *Remote Sensing* 14 (22): 5790. doi:10.3390/rs14225790.
- Watson, C. S., J. R. Elliott, S. K. Ebmeier, M. A. Vásquez, C. Zapata, S. Bonilla-Bedoya, P. Cubillo, et al. 2022. "Enhancing Disaster Risk Resilience Using Greenspace in Urbanising Quito, Ecuador." *Natural Hazards and Earth System Sciences* 22 (5): 1699–1721. doi:10.5194/nhess-22-1699-2022.
- Welsh, B. C., and D. P. Farrington. 2008. "Effects of Improved Street Lighting on Crime." *Campbell Systematic Reviews* 4 (1): 1–51. doi:10.4073/csr.2008.13.

- Zhao, M., C. Cheng, Y. Zhou, X. Li, S. Shen, and C. Song. 2022. "A Global Dataset of Annual Urban Extents (1992–2020) from Harmonized Nighttime Lights." *Earth System Science Data* 14 (2): 517–534. doi:[10.5194/essd-14-517-2022](https://doi.org/10.5194/essd-14-517-2022).
- Zheng, Q., Q. Weng, L. Huang, K. Wang, J. Deng, R. Jiang, Y. Ziran, and M. Gan. 2018. "A New Source of Multi-Spectral High Spatial Resolution Night-Time Light Imagery—JL1-3B." *Remote Sensing of Environment* 215: 300–312. doi:[10.1016/j.rse.2018.06.016](https://doi.org/10.1016/j.rse.2018.06.016).